Journal of Applied Polymer Science

Synergistic effect of carbon nanotubes and clay platelets in reinforcing properties of silicone rubber nanocomposites

Bratati Pradhan,[1] Saheli Roy,[1] Suneel Kumar Srivastava,[1] Anubhav Saxena[2]

[1]Department of Chemistry, Indian Institute of Technology, Kharagpur 721302, India

[2]Momentive Performance Materials Programs, GE India Technology Centre Pvt. Ltd, EPIP, Phase 2, Hoodi Village, Whitefield Road, Bangalore 560 066, India

Correspondence to: S. K. Srivastava (E-mail: sunit@chem.iitkgp.ernet.in)

ABSTRACT: Fine powders of montmorillonite (MMT)/multiwalled carbon nanotube (MWCNT) hybrids have been prepared by simple grinding of MWCNT with MMT in different weight ratios of MMT to MWCNT (10 : 1, 6 : 1, 3 : 1, 1 : 1, and 1 : 3) and characterized by wide-angle X-ray diffraction, field emission scanning electron microscopy, and transmission electron microscopy. These studies have established the formation of the exfoliated structures of MMT/MWCNT (1 : 1) hybrid, in which MWCNTs exist in the state of single nanotubes that are adsorbed and intercalated on the surface and in between the MMT nanoplatelets. The hybrid has subsequently been used as reinforcing nanofiller in the development of high-performance silicone rubber (SR) nanocomposites, and a remarkably synergistic effect of MMT and MWCNT on SR properties has been observed. The tensile strength of SR containing 1% w/w of the MMT/MWCNT (1 : 1) hybrid is improved by 215%, whereas the SR filled with MMT or MWCNT alone showed an improvement of 46 and 25%, respectively, over that of unfilled SR. In addition, SR/1 wt % MMT/MWCNT (1 : 1) nanocomposites also exhibit the maximum improvement in thermal stability corresponding to 10% weight loss by 70°C, crystallization and melting temperatures increased by 8 and 6°C as inferred from thermogravimetric analysis and differential scanning calorimetry, respectively. This approach is promising for the preparation of high-performance SR nanocomposites by using different dimension nanofillers together. © 2015 Wiley Periodicals, Inc. J. Appl. Polym. Sci. **2015**, *132*, 41818.

KEYWORDS: clay; graphene and fullerenes; nanotubes; properties and characterization; thermal properties

Received 27 June 2014; accepted 24 November 2014

DOI: 10.1002/app.41818

INTRODUCTION

Silicone rubber (SR) are one of the most important functional polymers, which have received considerable interest owing to their unique properties, e.g., excellent physical, chemical, and thermally stability; low glass transition temperature; clarity; biocompatibility; nonreactivity; and low surface energy. However, its low surface energy accounts for a lack of intermolecular interaction, providing poor mechanical strength of elastomers. Therefore, SR needs to be reinforced for majority of its applications.[1–3] In recent years, one-dimensional (1D) multiwalled carbon nanotubes (CNTs) are found to be an important filler in the development of high-performance polymer nanocomposites.[4–6] However, CNTs are poorly dispersed in many common organic solvents and polymeric matrix. Although this problem has been overcome by covalent functionalization,[7,8] it introduces the defective sites in the nanotubes, deteriorating the properties of CNTs as reinforcing filler in the formation of polymer nanocomposites.[7,8] Therefore, it remains a major challenge to find out simple ways and means to enhance the dispersion of CNTs in the development of polymer/CNT nanocomposites. Montmorillonite (MMT) is another two-dimensional (2D) inorganic material consisting of 2 : 1 layer structure with a central alumina octahedral sheet sandwiched in-between two silica tetrahedral sheets. However, it needs to be organomodified for its better dispersion as well as its compatibility in the fabrication of polymer nanocomposites.[9]

In very recent years, the hybridization of 1D nanotubes and 2D lamellar flakes to form MMT/CNT hybrid nanomaterials is more interesting owing to its versatile and tailormade properties than those of the individual materials.[10–14] These hybrids have been prepared by *in situ* growth of CNTs on clay layers[11–13] and wet mixing of organically modified CNTs and clay.[14] According to Lan and Lin,[10] the aggregation of CNT in various organic mediums (toluene, dimethylformamide, and ethanol) or in

Additional Supporting Information may be found in the online version of this article.

© 2015 Wiley Periodicals, Inc.

water is reduced by simply grinding it with MMT, mica, and layered double hydroxide (LDH). However, no significant work has further been reported using these as nanofillers in the formation of polymer nanocomposites. Inspired by this, we prepared the MMT/MWCNT hybrids by dry grinding and studied its structure by wide-angle X-ray diffraction (WAXD). Further, the field emission scanning electron microscopy (FESEM), atomic force microscopy (AFM), and transmission electron microscopy (TEM) studies have been carried out to unfold the morphology of prepared MMT/MWCNT hybrid fillers. MWCNTs applied in this work possess an aspect ratio in the range of 600–1000 and its hybridization with MMT is anticipated to improve the dispersion stability of hybrid. Subsequently, the prepared MMT/MWCNT hybrids have been used as filler to investigate the synergistic effect on mechanical and thermal properties of SR.

EXPERIMENTAL

Materials

Commercially available SR (Baysilone U10, vinyl content 0.05 mmol/g), vinyl-terminated, linear polydimethylsiloxane base polymer and Baysilone U crosslinking agent 430, and Pt catalyst complex were supplied by Momentive Performance Materials, Bangalore, India. Ethynyl cyclohexanol (inhibitor) and CNT, multiwalled 724769 (carbon > 95%, O.D × *L* 6–9 nm × 6 μm) were purchased from Sigma-Aldrich. Sodium montmorillonite (SWy-2) with cation exchange capacity "85 mequiv/100 g" was received from clay mineral repository, University of Missouri, Columbia. Chloroform ($CHCl_3$), toluene, tetrahydrofuran (THF), acetone, dimethylformamide (DMF), and ethanol were purchased from E. Merck, India.

Preparation of MMT/MWCNT Hybrid

MMT/MWCNT hybrids (10 : 1, 6 : 1, 3 : 1, 1 : 1, and 1 : 3 weight ratios) have been prepared by grinding the pristine MMT and MWCNT in an agate mortar and pestle for half an hour. To ensure the through mixing, the sides of the mortar were also occasionally scraped down with the pestle.

Preparation of SR Nanocomposites

The 1.0 wt % of MMT/MWCNT hybrids (10 : 1, 6 : 1, 3 : 1, 1 : 1, and 1 : 3 wt ratio) were mixed with vinyl-terminated, linear polydimethylsiloxane base polymer in THF by ultrasonication for 1 h. Then, the appropriate amounts of catalyst, inhibitor, and crosslinker (V430) with a 3 : 1 mole ratio of hydride (crosslinker) to the vinyl group of base polymer were added to the above mixture at room temperature. Finally, the resultant mixture was cast on a Teflon Petri dish and the solvent was removed at room temperature. Subsequently, the cast samples were cured at 165°C for 15 min followed by postcuring at 200°C for 4 h in a hot air oven. The same methodology was adopted for SR, SR/MMT, and SR/MMT/MWCNT (1 : 1) with different amount of hybrid materials (0.5, 0.75, 1, 1.5, and 2 wt %).

Characterization

WAXD patterns were collected at room temperature in the range of diffraction angle $2\theta = 3°–40°$ on a PANalytical (PW3040/60), model "X" pert pro with Cu Kα radiation ($\lambda = 0.1542$ nm) at a scanning rate of 3°/min. TEM analysis was recorded on JEOL 2100 TEM

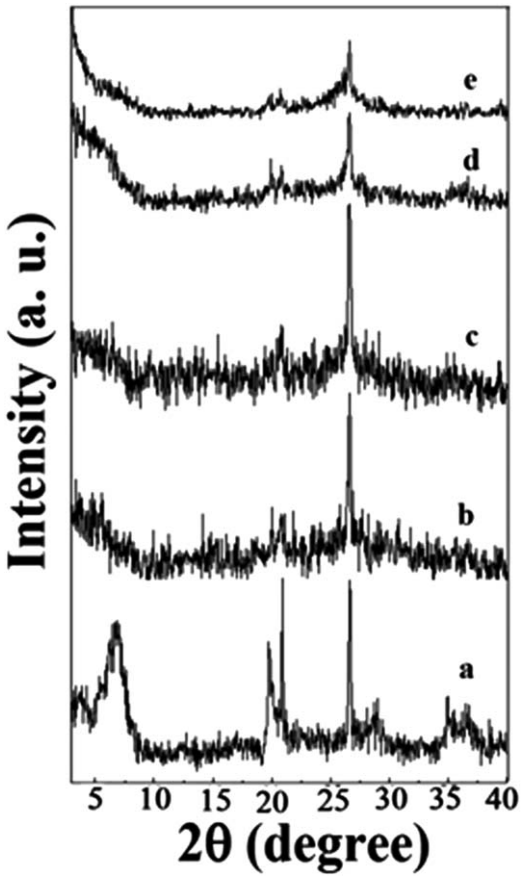

Figure 1. WAXD patterns of (a) MMT, (b) MMT/MWCNT (10 : 1), (c) MMT/MWCNT (6 : 1), (d) MMT/MWCNT (3 : 1), and (e) MMT/MWCNT (1 : 1) hybrids.

instruments operated under an acceleration voltage of 200 keV. For this purpose, samples were sonicated in THF following drop casting their dispersions on the carbon-coated copper grid. FESEM images were obtained on a Carl Zeiss Supra 40 instrument at an accelerating voltage of 20 kV. AFM analysis was performed on AFM (Digital Instruments, Nanoscope III) in tapping mode and scanned area was 5 μm × 5 μm. All the samples were prepared by spin coating of samples in silicon wafer. The samples for the tensile analysis were prepared according to ASTM D 412-98 standard and the measurements were performed using a Tinius Olsen h10KS universal testing machine at 25°C with a crosshead speed of 300 mm/min; dumbbell-shaped specimens with overall length of 100 mm and width of 3 mm. Six dumbbell-shaped specimens were punched for tensile testing. Differential scanning calorimetry (DSC) was performed using Perkin Elmer Pyris differential scanning calorimetric instrument at a scan rate of 10°C/min under nitrogen atmosphere over a range of temperature −150 to +150°C with a heating–cooling–heating cycle by taking 6 mg for all samples. Thermogravimetric analysis (TGA) of the SR films was conducted using Redcroft 870 thermal analyzer, Perkin-Elmer at a heating rate of 10°C/min over a temperature range of 50–800°C under nitrogen atmosphere.

RESULTS AND DISCUSSION

Figure 1 displays WAXD patterns of MMT and MMT/MWCNT hybrids in the 10 : 1, 6 : 1, 3 : 1, and 1 : 1 weight ratios. MMT

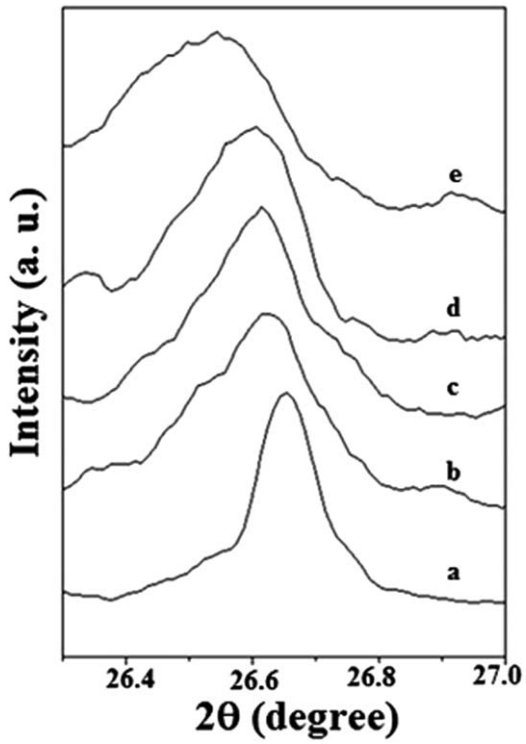

Figure 2. WAXD profiles for 101 reflection of (a) MMT, (b) MMT/MWCNT (10 : 1), (c) MMT/MWCNT (6 : 1), (d) MMT/MWCNT (3 : 1), and (e) MMT/MWCNT (1 : 1) hybrids.

shows the presence of a basal reflection peak (001) at $2\theta = 6.71°$ ($d_{001} = 1.31$ nm).[15] This observation is attributed to one layer of water molecule hydrated MMT, as reported earlier.[16] In addition, the diffraction peaks corresponding to 003, 100, and 101 reflections of chlorite and quartz existing as impurities are also observed at 19.81°, 20.79°, and 26.62°, respectively. However, peak at $2\theta = 6.71°$ corresponding to MMT disappeared indicating the exfoliation of its layers in the presence of MWCNT in MMT/MWCNT hybrids.[12] Further, a slow scan of the X-ray diffraction of 101 peaks present in MMT and MMT/MWCNT hybrids in Figure 2 shows a gradual shift as well as a broadening of the corresponding peak with decreasing concentration of MMT/MWCNT ratio. Furthermore, it is also observed that peaks are asymmetric at the lower angle than on the higher angle regions. It is well known that such asymmetric behavior of MMT peak in the presence of MWCNT could be attributed to the introduction of layer disorder in MMT.[17–19] Imperfection of crystallite as a result of lattice strain, dislocation, and stacking faults are also known to contribute toward the broadening of X-ray diffraction peak of MMT/MWCNT. Table I records the crystallite size of different MMT/MWCNT hybrids calculated on the basis of Scherrer equation.[18] In addition, dislocation density and microstrain have also been calculated[18,19] and presented in Table I. It is noted that MMT/MWCNT (1 : 1) exhibits lowest crystallite size, the dislocation density, and highest microstrain.

FESEM analysis has already been used as an important tool in establishing the morphology of hybrids prepared by the combination of 1D and 2D materials, e.g., MoS_2–MWCNT,[18] TiS_2–MWCNT,[19] MWCNT–graphene,[20] and LDH–graphene.[21] Figure 3 displays FESEM images of MMT and MWCNT–MMT hybrids prepared in various weight ratios. It is clearly evident that MMT exist as flakes with smooth surface with distinct bent edges. However, CNTs appear to be homogeneously dispersed among MMT flakes in MMT/MWCNT (3 : 1) and (1 : 1) hybrids. In addition, MWCNTs tend to protrude through the surfaces of MMT flakes (marked with arrow). Further, FESEM images of MMT/MWCNT (1 : 1) hybrid captured at a tilted angle (23°) show the formation of network between MMT platelets and MWCNTs leading to a 3D-like architecture. The formation of this network is likely to enhance the physicochemical properties of SR/MMT/MWCNT nanocomposites compared with neat SR and other hybrid-filled SR nanocomposites. FESEM image also showed that CNTs exist as aggregated bundles in MMT/MWCNT (1 : 3) hybrid in all probability owing to lowest interaction between the individual components.

The formation of MMT/MWCNT (1 : 1) hybrids has been further investigated by recording low- as well as high-magnification HRTEM images as shown in Figure 4. It is clearly seen that MMT and MWCNT co-exist together without any aggregation in MMT/MWCNT (1 : 1) hybrid. HRTEM images of MMT/MWCNT (1 : 1) hybrid also show that the CNTs are confined to surface of clay layers and also tend to bulge out through the surfaces of MMT sheets as indicated by the circle in the corresponding image. It is also evident that few MMT flakes are attached to the sidewalls of MWCNT as indicated by arrow in Figure 4. These images clearly suggested the formation of network structure in MMT/MWCNT (1 : 1) hybrid.[12] In addition, HRTEM images also show that the ratio of MMT/MWCNT has a significant influence on the dispersive characteristics. It is noted that the individual MWCNTs are evenly distributed in MMT/MWCNT (1 : 1) hybrid without any aggregation on the surface of negatively charged MMT platelets. In probability, there exists a strong interaction between negatively charged surface of MWCNTs and Na^+ ions present in MMT.[22] Alternatively, the presence of Na^+ ions acting as a counterion between MMT sheets and MWCNT facilitating the

Table I. Crystallite Size, Microstrain, and Dislocation Density of Pristine MMT and MMT/MWCNT Hybrids

Sample	Crystallite size (nm)	Microstrain	Dislocation density (line m^{-2})
MMT	74	4.71×10^{-4}	3.05×10^{10}
MMT/MWCNT(10 : 1)	38	9.24×10^{-4}	11.7×10^{10}
MMT/MWCNT(6 : 1)	36	9.54×10^{-4}	12.5×10^{10}
MMT/MWCNT(3 : 1)	34	1.013×10^{-3}	14.0×10^{10}
MMT/MWCNT(1 : 1)	30	1.149×10^{-3}	18.1×10^{10}

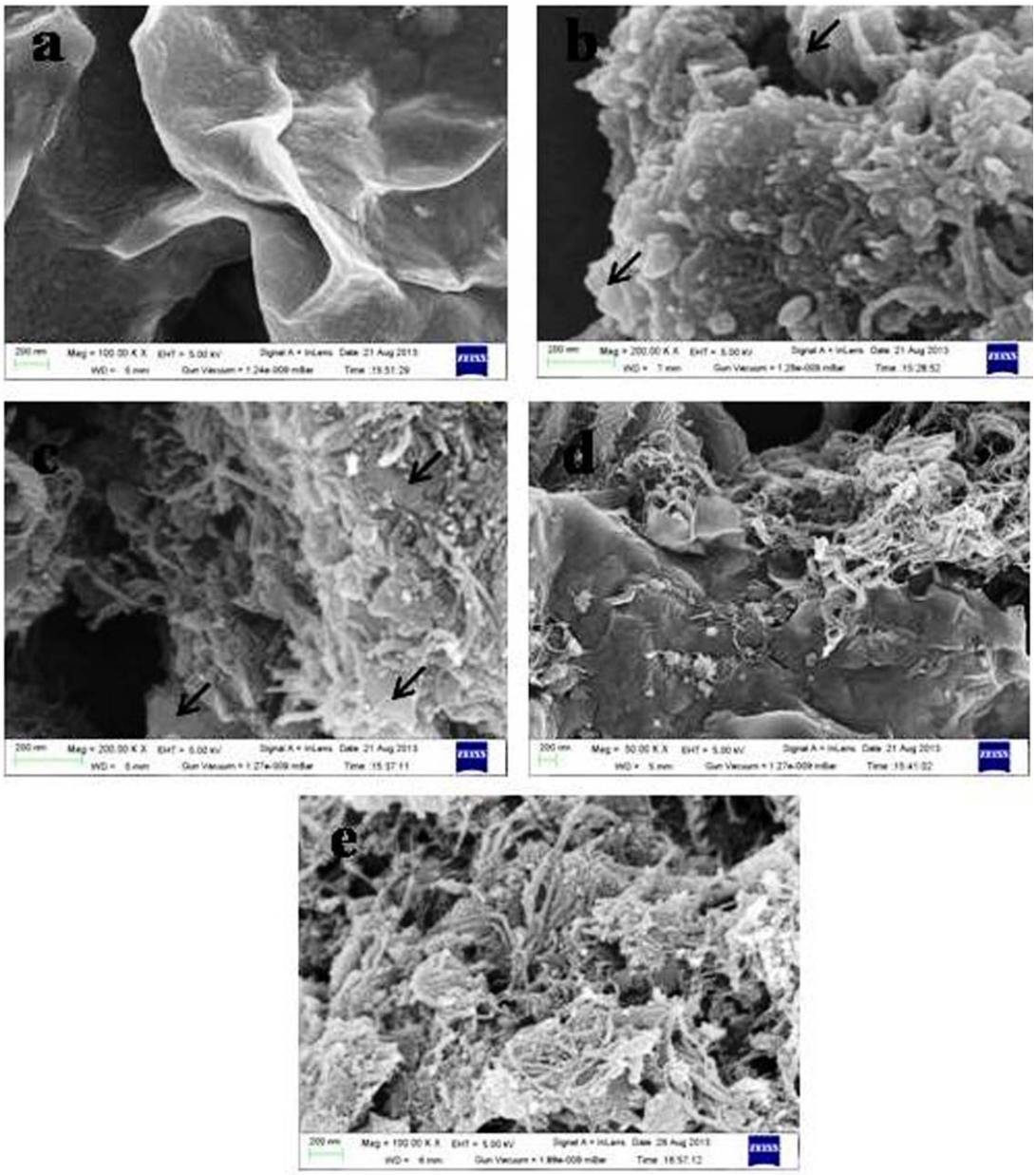

Figure 3. FESEM images of (a) MMT, (b) MMT/MWCNT (3 : 1), (c) MMT/MWCNT (1 : 1), (d) MMT/MWCNT (1 : 3), and (e) MMT/MWCNT (1 : 1) at a tilted angle of 23°. [Color figure can be viewed in the online issue, which is available at wileyonlinelibrary.com.]

formation of stable dispersions of MWCNT/MMT in THF also cannot be ruled out.[23]

The surface profile analysis of MMT has also been performed through AFM technique to further confirm the formation of three-dimensional (3D) network between MMT and MWCNT. AFM analysis has been carried out on MMT/MWCNT (1 : 1) hybrid. Figure 5 clearly indicates that MMT is present on the surface with MWCNT protruding in the third dimension (viz., *Z*-axis). The presence of such projections of MMT and MWCNT together confirmed the formation of 3D network in MMT/MWCNT (1 : 1) hybrid. It is also interesting to note that MWCNTs tend to project out homogenously through the surface of MMT platelets. In addition, 2D AFM image of MMT/MWCNT (1 : 1) hybrid in Figure 5 shows the presence of bright regions corresponding to MWCNTs, on the flat surface of MMT platelets. The section profile of the marked cross section in this image shows the variation in the height due to the MWCNT bulging out from the flat surface of MMT.

XRD, HRTEM, and AFM analysis, discussed earlier, clearly indicate that MMT/MWCNT (1 : 1) compared with other hybrids appears to be best in the preparation of SR nanocomposite. As a result, MMT/MWCNT (1 : 1) hybrid was selected as filler and studied its dispersion in most common solvents (DMF, THF, chloroform, toluene, acetone, and water). These qualitative findings have also been compared with respect to the dispersion of individual MWCNT and MMT fillers in the same solvents and

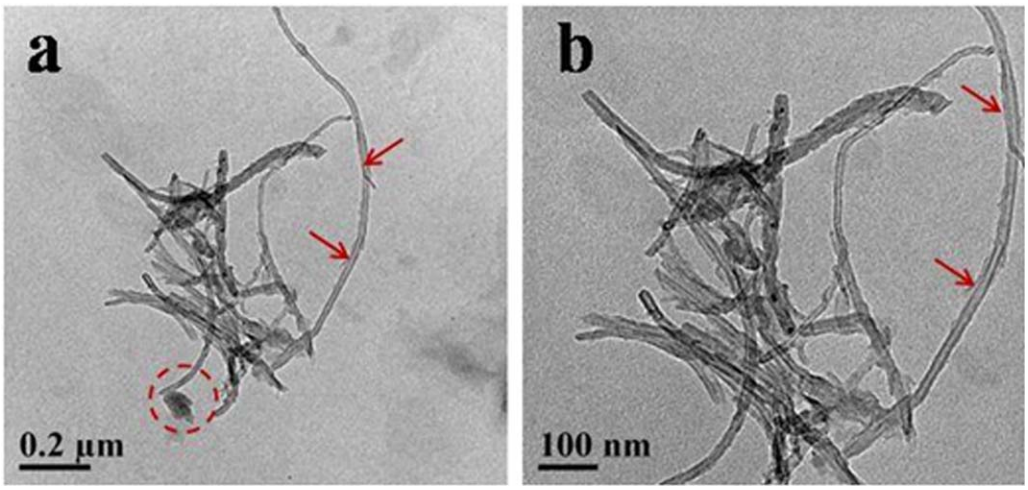

Figure 4. HRTEM images of MMT/MWCNT (1 : 1) hybrid at (a) low magnification and (b) high magnification (MMT flakes are indicated by arrows and circle). [Color figure can be viewed in the online issue, which is available at wileyonlinelibrary.com.]

the corresponding data are presented in Table II. It is found that MWCNTs are poorly dispersed in DMF and THF, but precipitates in chloroform, water, toluene, and acetone. In contrast, MMTs are swollen in water, but lack its dispersion in DMF, THF, chloroform, toluene, and acetone. However, MMT/MWCNT (1 : 1) hybrids are found to be easily dispersed with a mild sonication in all these solvents. These observations could be interpreted in terms of the charged nanoparticles or clusters attached on the surface of larger uncharged particle, imparting thereby the colloidal stability of the hybrid under the dominance of segregative Coulombic repulsions.[24,25]

Figure 6 shows WAXD analysis for SR and its composites containing 1 wt % of MMT, 1 wt % of MWCNT, and 0.5, 0.75, 1, 1.5, and 2 wt % of MMT/MWCNT (1 : 1). It is noted that SR exhibits two diffraction peaks at around $2\theta = 12.28°$ and 21.31° due to the amorphous nature of SR.[26,27] In case of SR/1 wt % MMT composite, the characteristic peaks of MMT appear owing to its aggregation. Interestingly, these characteristic peaks are

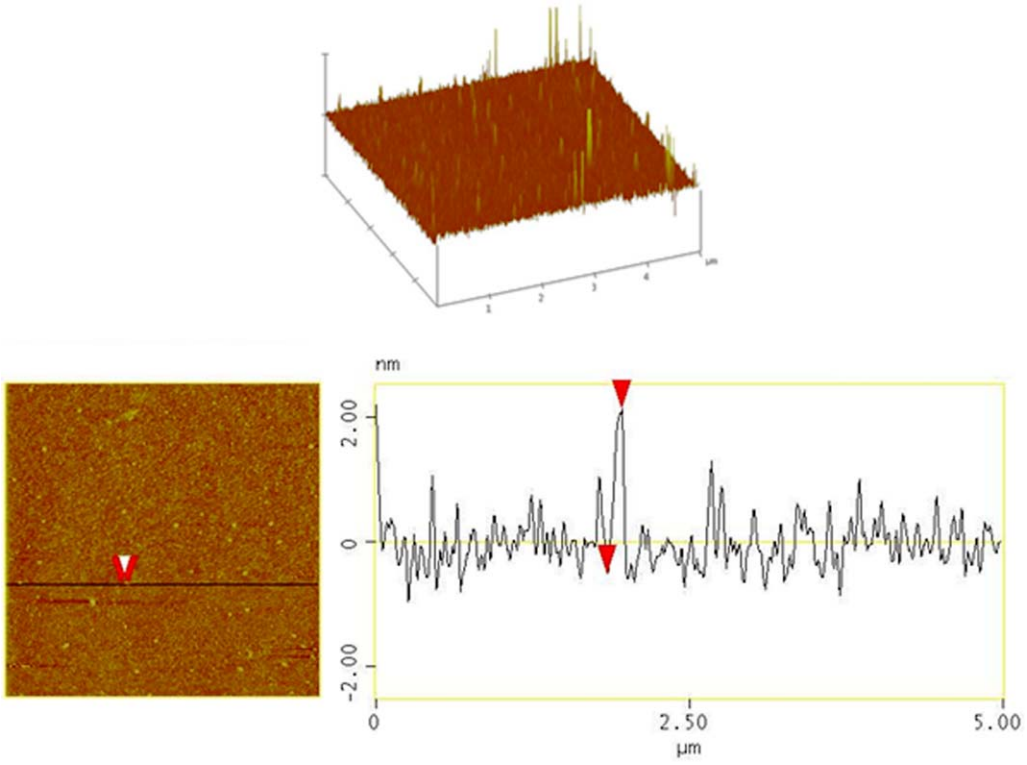

Figure 5. (a) Three-dimensional and (b) two-dimensional and corresponding section profile of AFM images of MMT/MWCNT (1 : 1) hybrid. [Color figure can be viewed in the online issue, which is available at wileyonlinelibrary.com.]

Table II. Dispersion of MMT, MWCNT, and MMT/MWCNT (1 : 1) Hybrids in Various Solvents

Solvent	MMT[a]	MWCNT[b]	MMT/MWCNT hybrid[c]
Water	Good dispersion	Precipitation	Good dispersion
Acetone	Precipitation	Precipitation	Good dispersion
Ethanol	Precipitation	Precipitation	Good dispersion
DMF	Precipitation	Poor dispersion	Good dispersion
THF	Precipitation	Poor dispersion	Good dispersion
Chloroform	Precipitation	Precipitation	Good dispersion
Toluene	Precipitation	Precipitation	Good dispersion

[a] MT, 0.1 mg in 1 mL.
[b] MWCNT, 0.1 mg in 1 mL.
[c] MMT/MWCNT hybrid (0.1 mg/0.1 mg) in 1 mL solvent for dispersion.

absent in 0.5, 0.75, 1, 1.5, and 2 wt % MMT/MWCNT (1 : 1)-filled nanocomposites of SR demonstrating the exfoliation of hybrid filler in SR matrix. The low-angle ($2\theta = 2$–$10°$) X-ray diffraction patterns provided in the inset of Figure 6 also show the disappearance of 001 basal peak in 1 and 2 wt % filled MMT/MWCNT (1 : 1). Figure 6 also shows that the broad diffraction peak position of SR remained more or less unaltered on incorporating MMT, MWCNT, and MMT/MWCNT as hybrid fillers. In addition, the full width at half maximum of SR diffraction peak ($2\theta \approx 12.28°$) in SR/MMT/MWCNT (1 : 1) nanocomposites is relatively low (2.80°–3.12°) compared with SR and its individually filled MMT and MWCNT composites with their corresponding values of 3.33°, 3.14–3.26°, and 3.12–3.20°, respectively. This clearly signifies the increasing ordering of SR chains in the presence of MMT/MWCNT (1 : 1) hybrids. This is possibly due to the interfacial interaction between the hybrid filler and SR,[28,29] which improves the properties of the corresponding nanocomposites.

TEM images of SR/0.5 wt % MMT, SR/0.5 wt % MWCNT, SR/1 wt % MMT/MWCNT (1 : 1), and SR/2 wt % MMT/MWCNT (1 : 1) nanocomposites are displayed in Figure 7(a–d), respectively. It is evident that MWCNT exists in the bundled form in its SR nanocomposite due to the presence of strong van der Waals force of attraction, whereas MMT nanoplatelets more or less maintained their stacking morphology, even in SR/MMT composites. Interestingly, MWCNTs are found to be dispersed as individual nanotubes at 1.0 wt % loading of MWCNT/MMT hybrid in SR. However, MMT could not be clearly located in SR/MWCNT/MMT possibly due to its smaller size of the dispersed MMT phase in nanocomposite.[14] But at higher MWCNT/MMT filler loading (2 wt %), well-dispersed MWCNT and full exfoliation of nanoclays can be observed. A part of CNT is indicated by black arrows and the MMT layers by red arrows, which could be attributed to the electrostatic attraction between MWCNT and MMT nanoplateletes.[14] In addition, the possibility of interaction through the hydrogen bonding between —OH group of MMT and —O— of SR accounting for the enhanced dispersion of the hybrid filler cannot be ruled out.[30]

The mechanical properties of SR have been investigated in the presence of 1 wt % filled MMT/MWCNT (1 : 3, 1 : 1, 3 : 1, 6 : 1, and 10 : 1 wt ratio) hybrids and shown in Figure 8. It is inferred that the tensile strength (TS) of SR (0.32 MPa) is improved maximum to 1.01 MPa in SR/MMT/MWCNT (1 : 1) nanocomposites. Figure 9 also shows the stress–strain plots for the nanocomposites of SR/MWCNT (0.5 wt %), SR/MMT (0.5 wt %), and SR/MMT (0.5 wt %)/MWCNT(0.5 wt %). The corresponding TS values with respect to SR are found to be 46, 25, and 215%, which confirmed the synergistic effect of MMT and MWCNT on SR. Further, tensile measurements on 0.5, 0.75, 1.0, 1.5, and 2 wt % of MMT/MWCNT (1 : 1)-filled SR nanocomposites have been carried out and the corresponding findings are displayed in Figure 10. These findings clearly show that TS is improved enough at all filler loadings in SR, although the maximum enhancement observed in 1 wt % MMT/MWCNT (1 : 1)-filled SR. Such improvements in the TS may be attributed to the random distribution of the hybrid nanofillers in SR matrix and strong interfacial interactions between the nanofillers and SR matrix to transfer the load from polymer matrix to hybrid.[11] Alternatively, there is a possibility of strong interaction between—OH (MMT)/—O—SR through hydrogen bonding. In addition, the larger aspect ratio of MWCNT and the higher surface area of MMT could lead to the formation of network in the SR due to these 1D and 2D fillers. Figure 11 also shows that elongation at break (EB) of SR gradually increases in the presence of MMT/MWCNT (1 : 1) hybrids and attains maximum value (260%) at its 1 wt % filler loading. This is in all probability due to the entanglement of polymer chain/synergistic effect

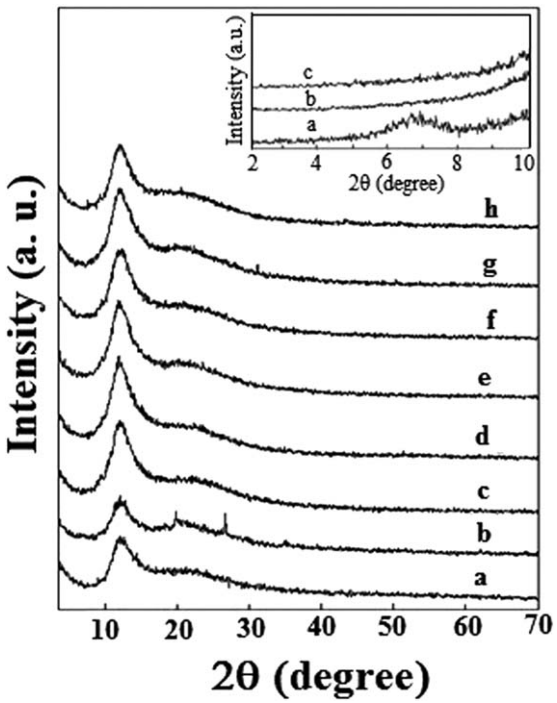

Figure 6. WAXD patterns of (a) SR, (b) SR/1 wt % MMT, (c) SR/1 wt % MWCNT, (d) SR/0.5 wt % MMT/MWCNT (1 : 1), (e) SR/0.75 wt % MMT/MWCNT (1 : 1), (f) SR/1 wt % MMT/MWCNT (1 : 1), (g) SR/1.5 wt % MMT/MWCNT (1 : 1), and (h) SR/2 wt % MMT/MWCNT (1 : 1) nanocomposites. Inset shows the low-angle XRD of (a) SR/1 wt % MMT, (b) SR/1 wt % MMT/MWCNT (1 : 1), and (c) SR/2 wt % MMT/MWCNT (1 : 1) nanocomposites.

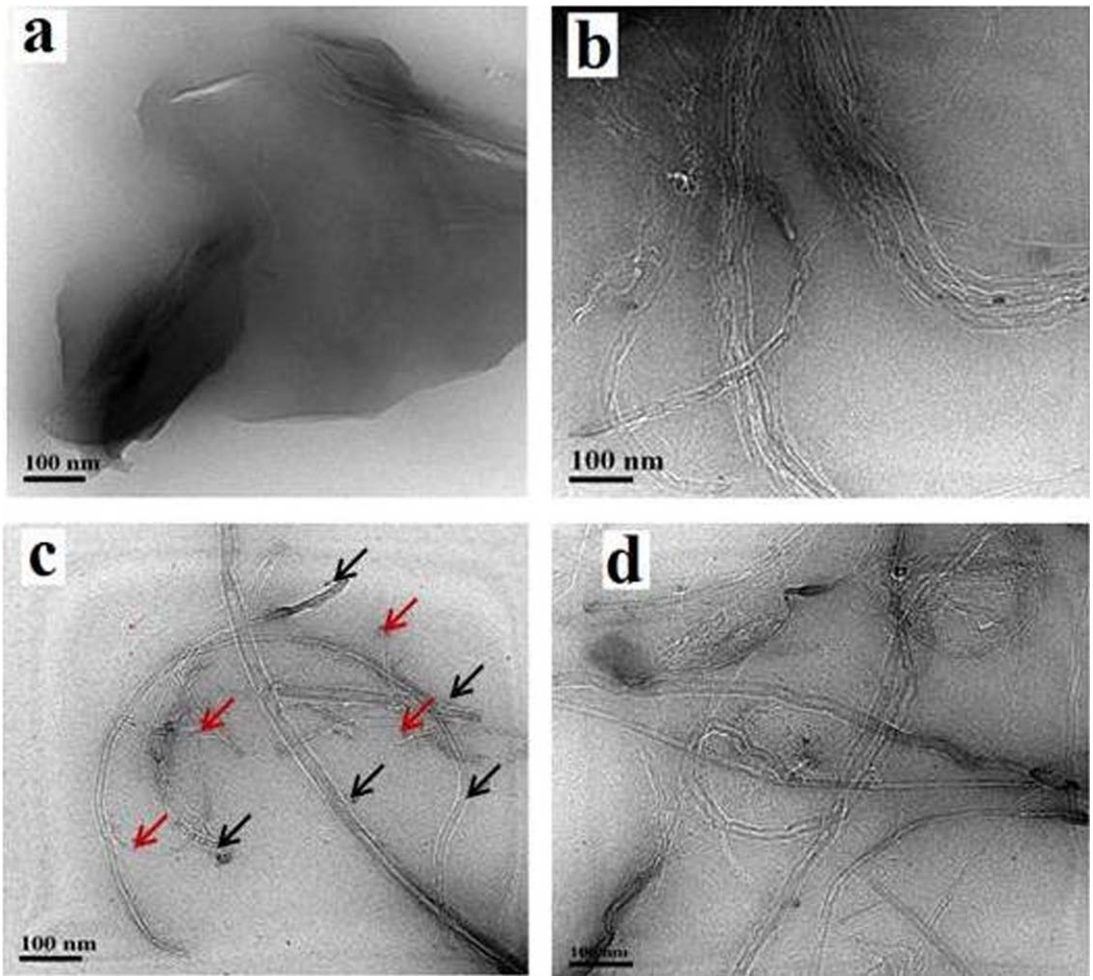

Figure 7. TEM image of (a) SR/0.5 wt % MMT, (b) SR/0.5 wt % MWCNT, (c) SR/1 wt % MMT/MWCNT (1 : 1), and (d) SR/2 wt % MMT/MWCNT (1 : 1) nanocomposites. [Color figure can be viewed in the online issue, which is available at wileyonlinelibrary.com.]

of chain slippage, platelet orientation of MMT, and deformation of the MWCNT.[31,32] However, TS and EB of SR decrease at higher filler loadings due to the aggregation tendency of the MMT/MWCNT. Interestingly, Young's modulus continuously increases with increasing wt % of hybrid filler, from 0.40 MPa (neat SR) to 1.1 MPa (SR/2 wt % MMT/MWCNT). This is

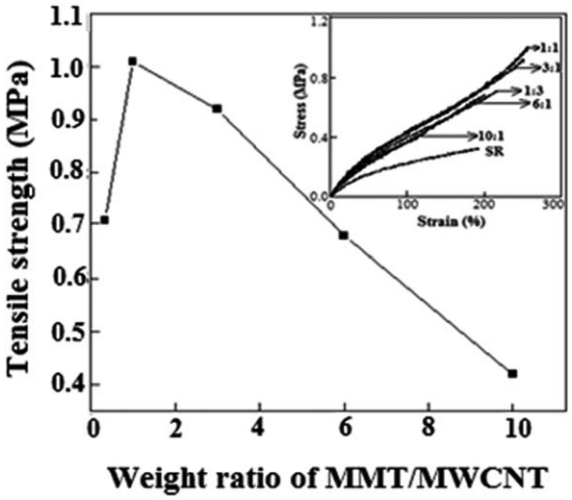

Figure 8. Variation of tensile strength of SR nanocomposites containing a particular (1 wt %) MMT/MWCNT in different weight ratios (10 : 1, 6 : 1, 3 : 1, 1 : 1, and1 : 3).

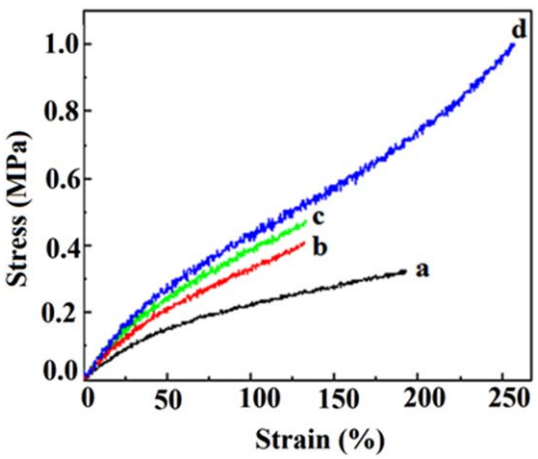

Figure 9. Typical stress–strain curves of (a) SR, (b) SR/0.5 wt % MMT, (c) SR/0.5 wt % MWCNT, and (d) SR/1 wt % MMT/MWCNT (1 : 1) nanocomposites. [Color figure can be viewed in the online issue, which is available at wileyonlinelibrary.com.]

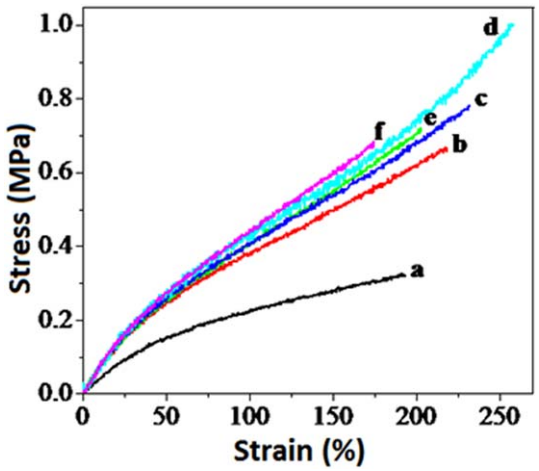

Figure 10. Stress–strain curves of (a) SR, (b) SR/0.5 wt % MMT/MWCNT (1 : 1), (c) SR/0.75 wt % MMT/MWCNT (1 : 1), (d) SR/1 wt % MMT/MWCNT (1 : 1), (e) SR/1.5 wt % MMT/MWCNT (1 : 1), and (f) SR/2 wt % MMT/MWCNT (1 : 1) nanocomposites. [Color figure can be viewed in the online issue, which is available at wileyonlinelibrary.com.]

more likely due to the formation of brittle composite compared to SR.[11] Alternatively, the possibility of the resistance exerted by the sterically hindered MMT/MWCNT hybrid surface itself and strong polymer filler interaction enhancing the Young's modulus also cannot be overruled.[31]

Table III records the comparisons of our mechanical data vis-a-vis reported on the other recently reported hybrid-filled SR nanocomposites. It is clearly evident that MMT/MWCNT hybrid-filled SR nanocomposites exhibit significantly improved TS, EB, and modulus in compared to 1.0 wt % loaded LDH (Li-Al-LDH, Co-Al-LDH, Mg-Al-LDH)/MWCNT,[21] and 0.75 and 1.0 wt % filled MWCNT/graphene nanocomposites of SR.[20]

The crystal structure and crystallinity of the polymer/polymer nanocomposites also play an important role in determining their mechanical properties. Therefore, DSC analysis has been performed to understand the crystallization and melting behavior of SR and its nanocomposites filled with MWCNT, MMT, and MMT/MWCNT (1 : 1) hybrid. These findings are displayed

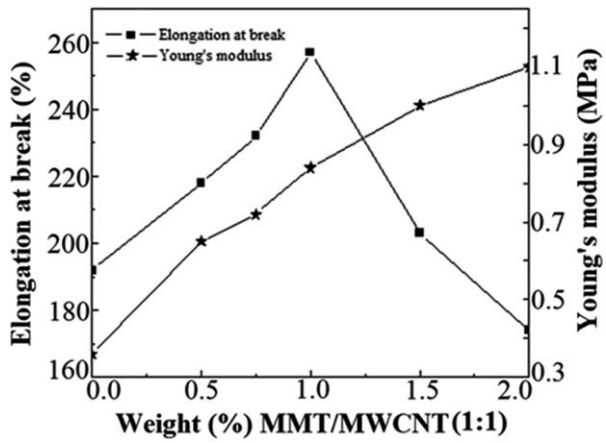

Figure 11. Variation of elongation at break (EB) and Young's modulus with MMT/MWCNT (1 : 1) hybrid contents of SR nanocomposites.

Table III. Mechanical Data Corresponding to Maximum Improvements in MMT/MWCNT/SR and Its Comparison with MWCNT–Graphene/VMQ[20] and LDH/MWCNT/SR[21]

Sample	TS (MPa)	EB (%)	Modulus (MPa)
SR	0.32	192	0.40
MMT/MWCNT/SR (1.0 wt %)	1.01	260	1.15
MWCNT/Graphene (0.75 wt %)/SR[20]	0.67	194	0.95
MWCNT/Graphene (1.5 wt %)/SR[20]	0.50	123	1.15
Li-Al-LDH/MWCNT (1.0 wt %)/SR[21]	0.68	190	
Mg-Al-LDH/MWCNT (1.0 wt %)/SR[21]	0.75	219	
Co-Al-LDH/MWCNT (1.0 wt %)/SR[21]	0.72	208	

in Supporting Information Figure S1 and the corresponding data are provided in Table IV. It is observed that the glass transition temperature (T_g) follows the order: SR < SR/MMT < SR/MWCNT < SR/MMT/MWCNT. The improvement in T_g of SR/MWCNT with respect to SR/MMT nanocomposite could be attributed to stronger interaction of MWCNT with SR owing to its higher available active surface. Interestingly, T_g of SR/MMT/MWCNT nanocomposite is improved (−123.72 to −124°C) with respect to neat SR (−129°C) due to restricted mobility of SR chains in the presence of hybrid filler.[33] The observed variation in T_g of the SR and its nanocomposites could be explained according to Flory–Fox equation,[34] The free volume between the polymer chains attains minimum value at T_g, consequently chain mobility reduces. When MMT/MWCNT filler is loaded in SR, these polymer chains tend to be aligned causing decrease in free volume and thereby increasing T_g of nanocomposites. It is also evident from Table IV that crystallization peak (T_c) is maximum enhanced in SR/1% MMT/MWCNT (−98.24°C) compared to neat SR (−106°C) due to heterogeneous nucleation effect of hybrid filler. In contrary, the crystallization peak is absent in SR, SR/MMT (0.5 and 1.0 wt %) in all probability due to the complete crystallization during their cooling.[35,36] Supporting Information Figure S1 also shows that the melting temperature (T_m) is maximum improved (−41°C) corresponding to 1.0 wt % MMT/MWCNT-filled SR compared with the neat SR (−46°C). This could be attributed to the strong interfacial interaction of MMT/MWCNT with SR, restricting the mobility of the polymer chains. Alternatively, there is a possibility that the presence of strong interaction between the hybrid filler and SR could orient polymer chains in regular manner and account for the observed increase in the crystallinity of SR nanocomposites.[37,38] Table IV also shows that ΔH_m remains nearly unaltered in individually filled SR composites, although it increased in corresponding SR/MMT/MWCNT composites. It is anticipated that the heterogeneous nucleation and crystallinity of SR in the presence of MMT/MWCNT hybrid nanofiller could also account for earlier observed improvement in the DSC analysis. The comparison of T_g, T_m, T_c, and ΔH_m values of SR/MMT/MWCNT (1 wt %) with recently reported work on 1 wt % filled MWCNT–graphene,[20] Li-Al-LDH/MWCNT,[21] Mg-Al-LDH/MWCNT,[21] and Co-Al-LDH/MWCNT[21] filled SR nanocomposites in Table IV clearly show that all the SR nanocomposites exhibit comparable improvements with respect to SR.

Table IV. Glass Transition Temperature (T_g), Melting Temperature (T_m), Crystallization Temperature (T_c), Enthalpy of Melting (ΔH_m), and Degree of Crystallinity (X_c) of Existing Work on SR, MMT/SR, MWCNT/SR, MWCNT/MMT/SR, and Its Comparison with MWCNT/Graphene/SR[20] and LDH/MWCNT/SR[21]

Sample	T_g (°C)	T_m (°C)	T_c (°C)	ΔH_m (J/g)	X_c (%)
SR	−129.00	−46.67	−106	22.054	58.920
SR/0.5% MMT	−127.00	−45.05	-	22.019	58.827
SR/1% MMT	−127.56	−47.14	-	22.004	58.787
SR/0.5% MWCNT	−126.05	−44.40	−100.57	21.049	56.235
SR/1% MWCNT	−126.41	−44.91	−99.76	20.065	53.606
SR/0.5% MMT/MWCNT	−125.56	−43.92	−99.24	23.002	61.453
SR/0.75% MMT/MWCNT	−123.72	−44.04	−99.10	23.414	62.554
SR/1% MMT/MWCNT	−124.00	−41.00	−98.24	24.373	65.116
SR/1.5% MMT/MWCNT	−125.69	−44.16	−99.71	23.355	62.396
SR/2% MMT/MWCNT	−125.84	−44.56	−100.02	23.088	61.683
MWCNT-Graphene (1.0 wt %)/SR[20]	−124.46	−41.81	−98	23.35	67.77
Li-Al-LDH/MWCNT (1.0 wt %)/SR[21]	−126.70	−44.78	−101.23	26.84	-
Mg-Al-LDH/MWCNT (1.0 wt %)/SR[21]	−124.00	−41.65	−98.05	28.23	-
Co-Al-LDH/MWCNT (1.0 wt %)/SR[21]	−126.49	−43.76	−97.88	27.42	-

Figure 12 represents TGA of SR and its nanocomposites filled with 0.5 wt % MMT, 0.5 wt % MWCNT, and 1 wt % MMT/MWCNT (1 : 1) hybrid in nitrogen atmosphere. The SR exhibited a sharp weight loss centered at 414°C, which corresponds to the depolymerization of the siloxane chains.[39] It is also evident from TGA that the weight loss is more pronounced in SR and SR/MMT compared to SR/MWCNT and SR/MMT/MWCNT nanocomposites. The onset decomposition temperatures of SR/MMT, SR/MWCNT, and SR/MMT/MWCNT nanocomposites are found to be 421, 429, and 447°C, respectively. Alternatively, when 10% weight loss is selected as a point of comparison, the respective thermal decomposition temperatures (T_{10}) for SR, SR/MMT, SR/MWCNT, and SR/MMT/MWCNT are 441, 463, 485, and 511°C, respectively. These findings clearly demonstrate that SR nanocomposites of MMT/MWCNT achieved a maximum improvement in thermal stability (by 70°C) than the SR or its individually filled MWCNT or MMT nanocomposites. According to recent reports, MWCNT–graphene (1.5 wt %) nanocomposite of SR[20] also exhibited maximum improvement in thermal stability (70°C) unlike that of 1 wt % loaded Li-Al-LDH/MWCNT/SR (14°C), Co-Al-LDH/MWCNT/SR (29°C), and Mg-Al-LDH/MWCNT/SR (44°C) nanocomposites.[21] This could be attributed to the hindering effect of the confined geometry originating from MWCNT and MMT together, where MWCNTs are inlaid between MMT nanoplatelets forming a sandwiched structure and wrapping around structure of hybrid filler by polymer chain through a strong interfacial interaction.

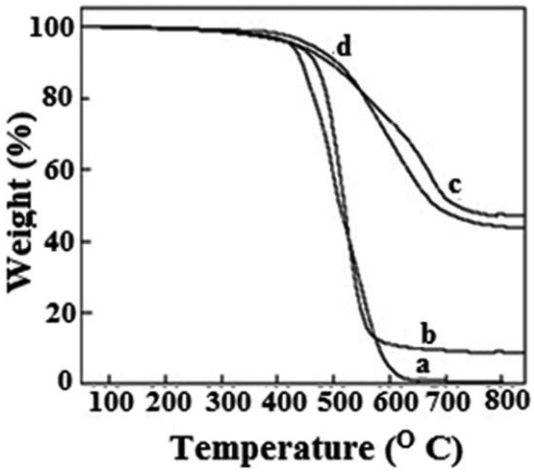

Figure 12. TGA curves of (a) SR, (b) SR/0.5 wt % MMT, (c) SR/0.5 wt % MWCNT, and (d) SR/1 wt % MMT/MWCNT (1 : 1) nanocomposites.

Interestingly, when 50% weight loss is selected as a point of comparison, the decomposition temperatures of SR, SR/MMT (0.5 wt %), SR/MWCNT (0.5 wt %), and SR/MMT/MWCNT (1 wt %) are found to be 510, 516, 705, and 678°C, respectively. This suggests that the decomposition temperature in general for the SR nanocomposite is relatively higher with respect to SR. It is also maximum improved for SR/MWCNT nanocomposite followed by MMT/MWCNT hybrid-filled SR. It is more likely that the sandwich structure of tetrahedral-octahedral-tetrahedral aluminosilicate of MMT plays an important role in understanding the degradation behavior either in SR/MMT or in SR/MMT/MWCNT. The earlier studies have shown that the dehydroxylation of MMT takes place above 450°C providing SiO_2 and Ai_2O_3,[40] which play a crucial role in the further degradation of SR.[41] Furthermore, the total residue left follows the order: SR (0.78%) < SR/MMT (8.8%) < SR/MMT/MWCNT (47.5%) < SR/MWCNT (44.6%). Interestingly, formation of such higher residue in SR/MWCNT and SR/MMT/MWCNT is nothing unusual. It is already reported that the high-temperature structural materials (silicon carbide, silicon carbonitride, and silicon oxycarbide) are produced, when the reactive filler particles are incorporated in the organosilicon precursors, such as

poly(carbosilanes), poly(silazane), or poly(sioxanes).[42] Very recently, Lopez-Manchado and coworkers[2] studied thermal behavior of the composite consisting of 0.5 wt % MWCNT-filled silicone foam and also observed a significant increase in the total residue (~48%) at 650–700°C. Alternatively, the higher thermal stability of in our SR/MWCNT and SR/MMT/MWCNT naocomposites could also be attributed to the formation of SiC_xO_y.[43]

CONCLUSION

MMT/MWCNT hybrids have been prepared by simple dry grinding of pristine MWCNT and MMT. WAXD demonstrated the formation of the hybrid, whereas TEM analysis shows that MWCNT and MMT both are completely exfoliated in MMT/MWCNT (1 : 1) in all probability due to stronger electrostatic interaction between MMT and MWCNT. These hybrids also exhibit the remarkable synergistic effect, when MMT/MWCNT (1 : 1) is used as reinforcing nanofillers in the SR nanocomposites. The TS and Young's modulus are found to be maximum improved to 215 and 133%, respectively, for 1 wt % MMT/MWCNT (1 : 1) loading in comparison to SR due to the homogeneous dispersion and strong interfacial interaction between SR and MMT/MWCNT hybrid. Thermal stability corresponding to 10% weight loss, crystallization temperature, and melting temperature of SR/1 wt % MMT/MWCNT (1 : 1) nanocomposite is found to be maximum improved by 70, 8, and 6°C, respectively, with respect to SR. It is expected that the SR/1 wt % MMT/MWCNT (1 : 1) nanocomposite with these significantly improved properties can have broader implications for other elastomeric-filled systems and could also be useful in manufacturing of the medical devices and aerospace/aircraft applications. The observed improvements in the properties of SR are also desirable for its outdoor insulation applications and need further investigation.

ACKNOWLEDGMENTS

The authors are grateful to CSIR and DRDO, New Delhi, India, for the financial support. They also thank Prof. S.K. Roy, Ms Susnata Bera (Department of Physics and Meteorology), and Prof. S. Das (Metallurgical and Materials Engineering) of Indian Institute of Technology, Kharagpur, for AFM and FESEM of the samples, respectively.

REFERENCES

1. Srivastava, S. K.; Pradhan, B. Concise Encyclopedia of High Performance Silicones; Wiley-Scrivener: Canada, **2014**; p 85.
2. Verdejoa, R.; Saiz-Arroyo, C.; Carretero-Gonzalez, J.; Barroso-Bujans, F.; Rodriguez-Perez, M. A.; Lopez-Manchadoa, M. A. *Eur. Polym. J.* **2008**, *44*, 2790.
3. Pradhan, B.; Srivastava, S. K.; Bhowmick, A. K.; Saxena, A. *Polym. Int.* **2012**, *61*, 458.
4. Bilotti, E.; Zhang, R.; Deng, H.; Baxendale, M.; Peijs, T. *J. Mater. Chem.* **2010**, *20*, 9449.
5. Raja, M.; Ryu, S. H.; Shanmugharaj, A. M. *Eur. Polym. J.* **2013**, *49*, 3492.
6. Wei, C.; Dai, L.; Roy, A.; Tolle, T. B. *J. Am. Chem. Soc.* **2006**, *128*, 1412.
7. Tchoul, M. N.; Ford, W. T.; Lolli, G.; Resasco, D. E.; Arepall, S. *Chem. Mater.* **2007**, *19*, 5765.
8. Williams, K. A.; Veenhuizen, T. M.; Torre, G.; Eritja, R.; Dekker, C. *Nature* **2002**, *420*, 76.
9. Pramanik, M.; Srivastava, S. K.; Samantaray, B. K.; Bhowmick, A. K. *J. Appl. Polym. Sci.* **2003**, *87*, 2216.
10. Lan, Y. F.; Lin, J. J. *J. Phys. Chem. A* **2009**, *113*, 8654.
11. Zhang, C.; Tjiu, W. W.; Liu, T.; Lui, W. Y.; Phang, I. Y.; Zhang, W. D. *J. Phys. Chem. B* **2011**, *115*, 3392.
12. Zhang, W. D.; Phang, I. Y.; Liu, T. *Adv. Mater.* **2006**, *18*, 73.
13. Liu, L.; Grunlan, J. C. *Adv. Funct. Mater.* **2007**, *17*, 2343.
14. Wang, Z.; Meng, X.; Li, J.; Du, X.; Li, S.; Jiang, Z.; Tang, T. *J. Phys. Chem. C* **2009**, *113*, 8058.
15. Chipera, S. J.; Bish, D. L. *Clays Clay Miner.* **2001**, *49*, 398.
16. Li, Z.; Kolb, V.; Jiang, W.-T.; Hong, H. *Clays Clay Miner.* **2010**, *58*, 462.
17. Srivastava, S. K.; Pramanik, M.; Palit, D.; Mathur, B. K.; Kar, A. K.; Samanta, R. B. K.; Haeuseler, H.; Cordes, W. *Chem. Mater.* **2001**, *13*, 4342.
18. Bindumadhavan, K.; Srivastava, S. K.; Mahanty, S. *Chem. Commun.* **2013**, *49*, 1823.
19. Bindumadhavan, K.; Srivastava, S. K.; Mahanty, S. *J. Nanopart. Res.* **2013**, *15*, 1950.
20. Pradhan, B.; Srivastava, S. K. *Polym. Int.* **2014**, *63*, 1219.
21. Pradhan, B.; Srivastava, S. K. *Composites Part A* **2014**, *56*, 299.
22. Sun, D.; Everett, W. N.; Chu, C. C.; Sue, H. *J. Small* **2009**, *5*, 2692.
23. Qiao, R.; Aluru, N. R. *Nano Lett.* **2003**, *3*, 1013.
24. Tohver, V.; Chan, A.; Sakurada, O.; Lewis, J. A. *Langmuir* **2001**, *17*, 8414.
25. Bourlinos, A. B.; Georgakilas, V.; Zboril, R.; Dallas, P. *Carbon* **2007**, *45*, 2136.
26. Albouy, P. A. *Polymer* **2000**, *41*, 3083.
27. Out, G. J. J.; Turetskii, A. A.; Snijder, M.; Moller, M.; Papkov, V. S. *Polymer* **1995**, *36*, 3213.
28. Sahoo, N. G.; Cheng, H. K. F.; Caia, J.; Li, L.; Chan, S. H.; Zhao, J.; Yu, S. *Mater. Chem. Phys.* **2009**, *117*, 313.
29. Chakoli, A. N.; Sui, J.; Amirian, M.; Cai, W. *J. Polym. Res.* **2011**, *18*, 1249.
30. Tang, C.; Xiang, L.; Su, J.; Wang, K.; Yang, C.; Zhang, Q.; Fu, Q. *J. Phys. Chem. B* **2008**, *112*, 3876.
31. Acharya, H.; Srivastava, S. K.; Bhowmick, A. K. *Compos. Sci. Technol.* **2007**, *67*, 2807.
32. Wu, Y. P.; Ma, Y.; Wang, Y. Q.; Zhang, Q. L. *Macromol. Mater. Eng.* **2004**, *289*, 890.
33. Rajesh, G.; Maji, P. K.; Bhattacharya, M.; Choudhury, A.; Roy, N.; Saxena, A.; Bhowmick, A. K. *Polym. Polym. Compos.* **2010**, *19*, 469.
34. Wall, L. A. *J. Res. Natl. Bur. Stand.* **1974**, *78A*, 447.

35. Dollase, T.; Wilhelm, M.; Spiess, H. W.; Yagen, Y.; Yerushalmi-Rozen, R.; Gottlieb, M. *Interface Sci.* **2003**, *11*, 199.

36. Dollase, T.; Spiess, H. W.; Gottlieb, M.; Yerushalmi-Rozen, R. *Europhys. Lett.* **2002**, *60*, 390.

37. Rim, P. B.; Runt, J. P. *Macromolecules* **1984**, *17*, 1520.

38. Farrow, G. *Polymer* **1963**, *4*, 191.

39. Camino, G.; Lomakin, S. M.; Lageard, M. *Polymer* **2002**, *43*, 2011.

40. Uhl, F. M.; Davuluri, S. P.; Wong, S. C.; Webster, D. C. *Chem. Mater.* **2004**, *16*, 1135.

41. Homma, H.; Kuroyagi, T.; IIzumi, K.; Mirley, C. L.; Ronzello, J.; Boggs, S. A. *Electr. Insul. Mater.* **1998**, *1*, 631.

42. Greil, P. *J. Am. Ceram. Soc.* **1995**, *78*, 835.

43. Radovanovic, E.; Gozzi, M. F.; Goncalves, M. C.; Yoshida, I. V. P. J. *Non-Cryst. Solids* **1999**, *248*, 37.